ChemPubSoc Europe

DOI: 10.1002/open.201900194

Open Access ChemistryOPEN Full Papers

Mechanochemical Preparations of Anion Coordinated Architectures Based on 3-Iodoethynylpyridine and 3-Iodoethynylbenzoic Acid

Vincent M. Morin, Patrick M. J. Szell, Estelle Caron-Poulin, Bulat Gabidullin, and David L. Bryce*[a]

The halogen bond has previously been explored as a versatile tool in crystal engineering and anion coordination chemistry, with mechanochemical synthetic techniques having been shown to provide convenient routes towards cocrystals. In an effort to expand our knowledge on the role of halogen bonding in anion coordination, here we explore a series of cocrystals formed between 3-iodoethynylpyridine and 3-iodoethynylbenzoic acid with halide salts. In total, we report the single-crystal X-ray structures of six new cocrystals prepared by mechanochemical ball milling, with all structures exhibiting C≡C–I···X$^-$ (X = Cl, Br) halogen bonds. Whereas cocrystals featuring a pyridine group favoured the formation of discrete entities, cocrystals featuring a benzoic acid group yielded an alternation of halogen and hydrogen bonds. The compounds studied herein were further characterized by ^{13}C and ^{31}P solid-state nuclear magnetic resonance, with the chemical shifts offering a clear and convenient method of identifying the occurrence of halogen bonding, using the crude product obtained directly from the mechanochemical ball milling. Whereas the ^{31}P chemical shifts were quickly able to identify the occurrence of cocrystallization, ^{13}C solid-state NMR was diagnostic of both the occurrence of halogen bonding and of hydrogen bonding.

1. Introduction

The structural features of a crystalline framework can be modified in order to exhibit desirable properties, such as porosity[1,2] and conductivity.[3,4] The design of such modifications within the context of crystal engineering has gained popularity in recent years,[5,6] following a rational design approach rather than using brute force. Cocrystals, which typically combine two or more components interacting by means of non-covalent interactions,[7,8] are a particular focus in the field of crystal engineering. Rather than forming and breaking covalent bonds, structures can be tuned by individually modifying each component of the cocrystal, potentially reducing screening times. Several synthetic processes have been proposed to prepare cocrystals, such as mechanochemistry,[9,10,11] and more recently, cosublimation,[12] yielding the final product in as little as 10 minutes, all without the need for large solvent volumes.

Halogen bonding has been shown to be a powerful tool for crystal engineering.[13,14] Halogen bonding, akin to hydrogen bonding,[15] is the attractive interaction between the region of increased electrostatic potential and reduced electron density[16] associated with a covalently bonded halogen, the σ-hole on the halogen bond donor,[17,18] and a nucleophile, named the halogen bond acceptor.[19] The favourable characteristics of the halogen bond can be attributed to the strength of the interaction, varying with the size of the halogen (I > Br > Cl ≫ F),[20] and the presence of an electron withdrawing group.[21] Iodine-substituted sp-hybridized carbons, as found in the iodoacetylene functional group, are among the most activated halogen bond donors,[22] offering the potential to form strong halogen bonds. As a result, reports featuring halogen bonds to iodoacetylene groups have gained momentum due to potential applications in crystal engineering.[23,24,25,26,27,28,29,30,31]

Halogen bonding has become an important interaction for anion coordination (C–I···X; X=Cl$^-$, Br$^-$, I$^-$),[32] offering directional scaffolding for crystal engineering. Several crystal structures have been reported featuring anions coordinated by halogen bond donors, such as 1,4-diiodotetrafluorobenzene[33,34] and 1,3,5-tri(iodoethynyl)-2,4,6-trifluorobenzene.[35,36] This C–I···X$^-$ motif has been shown to be of use in several classes of functional materials, such as in halide recognition[37] and rotaxanes.[38] The preparation of cocrystals bearing the C–I···X$^-$ halogen bonding motif by mechanochemistry has been previously exploited, offering the advantage of reduced preparation times.[39,40,41,42] In order to characterize the products, solid-state NMR (SSNMR) boasts the capability of offering structural information, such as identifying the occurrence of halogen

[a] V. M. Morin, Dr. P. M. J. Szell, E. Caron-Poulin, Dr. B. Gabidullin, Prof. Dr. D. L. Bryce
Department of Chemistry and Biomolecular Sciences
University of Ottawa
10 Marie Curie Private
Ottawa, Ontario K1N 6N5
Canada
Tel: +1-613-562-5800 ext.2018
fax: +1-613-562-5170
E-mail: dbryce@uottawa.ca

Supporting information for this article is available on the WWW under https://doi.org/10.1002/open.201900194

bonding, and has been also shown to be useful in ensuring phase purity.[12]

We have previously investigated two iodoethynyl halogen bond donors: 3-iodoethynylpyridine (**1**)[43] and 3-iodoethynylbenzoic acid (**2**).[44] The previously reported crystal structure of **1** includes a self-complimentary zig-zag framework *via* C–I···N halogen bonds, while its halide salts favoured discrete charged dimers *via* C–I···X^- halogen bonding and N–H···X^- hydrogen bonding. In contrast, the structure of **2** displays simultaneous C–I···C halogen bonding and O–H···O hydrogen bonding. Moreover, upon the cocrystallization of **2** with a series of nitrogen-containing heterocycles, the resulting frameworks featured both C–I···N halogen bonds and O–H···O or O–H···N hydrogen bonds. Here, we turn our attention to investigate the potential of **1** and **2** in anion coordination using a series of halide salts as the halogen bond acceptors. The molecular structures are shown in Figure 1. We employ a mechanochemical approach to

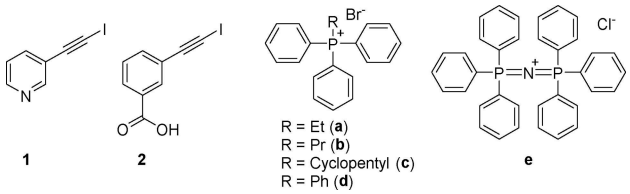

Figure 1. Molecular diagrams of the halogen bond donors (**1**, **2**) and the halide salts (**a**–**e**) used in this study. The R group denotes the substituent (ethyl, propyl, cyclopentyl, and phenyl).

screening cocrystals, and use ^{13}C and ^{31}P SSNMR to identify successful preparations, resulting in a notable decrease in overall discovery time.

Experimental Section

3-ethynylbenzoic acid (95%), silver nitrate (99%), 3-ethynylpyridine (98%), ethyltriphenylphosphonium bromide (99%), tetraphenylphosphonium bromide (97%), propyltriphenylphosphonium bromide (98%), and potassium iodide (99%) were purchased from Sigma Aldrich. N-iodosuccinimide (97%), bis(triphenylphosphoranylidene)ammonium chloride (97%), cyclopentyltriphenylphosphonium bromide (98%) and *tert*-butyl hydroperoxide (70% aq. solution) were purchased from Alfa Aesar. Reagent grade acetone and acetonitrile were purchased from Fisher Scientific. All compounds were used without further purification. Both **1** and **2** were prepared from 3-ethynylpyridine and 3-ethynylbenzoic acid following literature procedures.[43,44] The mechanochemical preparation of each of the cocrystals was performed using a Retsch MM400 ball mill. Both the halogen bond donor (**1**, **2**) and the appropriate halide salt (**a**–**e**) were added as powders successively to a 10 mL stainless steel milling jar in their proper stoichiometric ratio. All experimental masses and ratios can be found in Table S1 of the Supporting Information. Ball milling was performed with a milling frequency of 25 Hz for a period of 30 minutes at room temperature using two stainless steel grinding balls, in the presence of 10% M/M of acetonitrile. Crystals suitable for single crystal X-ray experiments were grown by dissolving the product obtained by ball milling in a minimum of acetonitrile, and allowing the solution to slowly evaporate. The phase purity of each compound was verified by powder X-ray diffraction on a Rigaku Ultima IV instrument with 2θ ranging from 5° to 55° at a rate of 1° per minute using CuKα radiation. All powder X-ray diffractograms can be found in the Supporting Information.

^{13}C Solid-State NMR Spectroscopy

All ^{13}C cross-polarization magic-angle spinning (CP/MAS) solid-state NMR experiments were performed at 9.4 T ($\nu_L(^{13}C) = 100.6$ MHz) using a Bruker 4 mm HXY probe and a Bruker Avance III NMR spectrometer. $^1H \rightarrow ^{13}C$ CP was used with a 3.6 µs proton $\pi/2$ pulse, a 2000 µs contact time, a recycle delay of 10 s, and a 69 kHz ^1H decoupling frequency. ^{13}C chemical shifts were referenced to glycine at 176.6 ppm ($^{13}C{=}O$) relative to tetramethylsilane (TMS). Variable spinning speeds were used to separate the spinning sidebands from the isotropic peaks. Further information, such as spinning speeds and the number of transients, can be found in the Supporting Information.

^{31}P Solid-State NMR Spectroscopy

All ^{31}P cross-polarization magic-angle spinning (CP/MAS) solid-state NMR experiments were performed at 4.7 T ($\nu_L(^{31}P) = 80.961$ MHz) using a Bruker 7 mm HXY probe and a Bruker Avance III NMR spectrometer. $^1H \rightarrow ^{31}P$ CP was used with a 3.75 µs proton pulse $\pi/2$ pulse, a 2000 µs contact time, and a 66.6 kHz ^1H decoupling frequency. ^{31}P chemical shifts were referenced to ammonium dihydrogen phosphate at 0.81 ppm. The MAS speed was set to 4 kHz. Some additional spectra acquired at 9.4 T are given in the Supporting Information.

Single Crystal X-Ray Diffraction

The crystals were mounted on thin glass fibers using paraffin oil. Prior to data collection, crystals were cooled to 200 ± 2 K. The data were collected on a Bruker AXS single crystal diffractometer equipped with a sealed Mo tube source (wavelength 0.71073 Å) and an APEX II CCD detector. The raw data collection and processing were performed with the Bruker APEX II software package.[45] Semi-empirical absorption corrections based on equivalent reflections were applied.[46] Systematic absences in the diffraction dataset and unit cell parameters were consistent with triclinic $P\bar{1}$ (#2) for **1a**, monoclinic $P2_1/n$ (#14) for **2b**, **2e**, monoclinic $P2_1/c$ (#14) for **1e**, orthorhombic *Pnma* (#62) for **2c**, and tetragonal $P\bar{4}2_1m$ (#113) for **1b**. The structures were solved by direct methods and refined with full-matrix least-squares procedures based on F^2, using SHELXL[47] and WinGX.[48] All non-hydrogen atoms were refined anisotropically. The hydrogen atoms bonded to the oxygen atoms (**1e**, **2b**, **2e**) were located in the difference Fourier map and refined freely (**2b**, **2e**) or with certain restraints (**1e**) while the remaining hydrogen atoms were placed in idealized positions. Displacement ellipsoid plots were produced using ORTEP[49] (see the Supporting Information), and uncertainties were estimated using PLATON for Windows.[50] The structure of **1a** was refined without any additional restraints or constraints. In **1b** the 3-iodoethynylpyridine molecule lies on a mirror plane and its occupation is conventionally constrained at 0.5. The tetraphenylphosphonium cation lies on a 4-fold rotoinversion axis with the P atom on the inversion center; therefore, the P atom has a fixed 0.25 occupancy and the phenyl group is fully occupied. The Br anion lies on an intersection of two mirror planes; its occupancy is 0.25. In **1e**, both water molecules were refined using 1,2-distance (bond length) and 1,3-distance (bond angle) restraints (DFIX in SHELXL). The U_{iso} for H(1 A), H(1B), H(2 A), H(2B) atoms were constrained at $1.5U_{eq}$ of the corresponding O atoms. In **2b** and **2e**, the H atoms of the

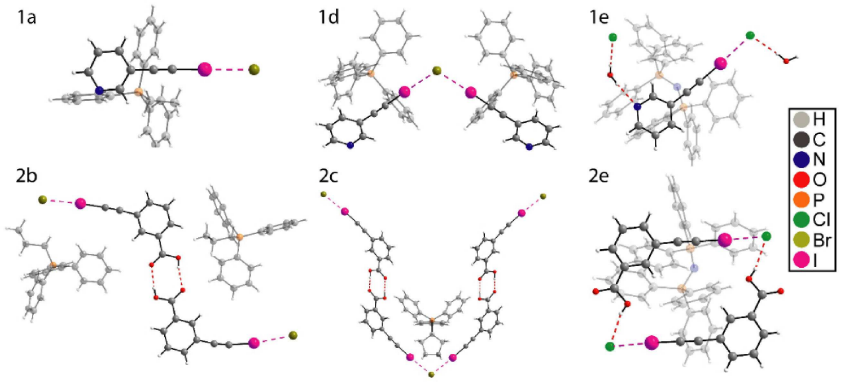

Figure 2. Depiction of the halogen and hydrogen bonding motifs in the crystal structures studied herein. The counterion is rendered transparent for clarity, highlighting the halogen/hydrogen bonding motifs. See text for further discussion.

carboxyl groups were refined freely without distance restraints nor ADP constraints. In **2c** the H(1A) atom of the carboxyl group was refined freely without distance restraints nor ADP constraints. The (cyclopentyl)triphenylphosphonium cation is located on a mirror plane. The C(10)..C(15) phenyl ring is fully occupied and the P atom lies directly on the mirror plane and has a half occupancy. One of the three phenyl groups (two positions: C(16)..C(19) and C(20′)..C(23′)) and the cyclopentyl group (two positions: C(20)..C(22) and C(16′)..C(18′)) are disordered over two mutually overlapping positions with 0.568(9):0.432(9) occupancies. These disordered fragments were refined using a number of restraints due to the complexity of the case: bond distance restraints (SADI and DFIX in SHELXL), a planarity restraint (FLAT in SHELXL) applied to the P(1),C(16)..C(19) and P(1),C(20′)..C(23′) fragments, an 'equal ADP' (EADP in SHELXL) constraint applied to the C(16),C(16′) and C(20),C(20′) atom pairs due to their spatial proximity and overlap, enhanced rigid-bond restraints (RIGU in SHELXL) applied to the ADPs of the P(1),C(16)..C(19), and P(1),C(16′)..C(18′), and P(1),C(20)..C(22), and P(1),C(20′)..C(23′) atom groups.

2. Results and Discussion

2.1. X-Ray Crystallography

Mechanochemical ball milling yielded crystalline powdered products in all cases. Following their identification by SSNMR (*vide infra*), a small portion of each product was subsequently dissolved and recrystallized by slow solvent evaporation in order to obtain crystals suitable for single crystal X-ray diffraction. A total of six X-ray crystal structures are reported here, with each structure exhibiting an iodine halogen bond to the anion of the halide salt (see Figure 2). Three structures feature **1** as the halogen bond donor, while the other three structures feature **2** as the halogen bond donor. The size of the cation in the salts varies, featuring short alkyl chains (**a**, **b**), rings (**c**, **d**), and finally a large cation (**e**). The purpose of these modifications was to relate the structural changes of the cation to the halogen bonding motif.

Structure **1a** reveals a single C–I···Br$^-$ halogen bond between **1** and the bromide anion of **a** ($d_{I\cdots Br}$ = 3.1344(9) Å, $\theta_{C\text{-}I\cdots Br}$ = 171.12(10)°), forming a discrete halogen bonded entity rather than a continuous framework. In addition to the halogen bond, the bromide anion is engaged in several short H···Br contacts involving both the phosphonium cation of **a** and the proton in the *para* position relative to the nitrogen of the pyridine ring of **1**, encapsulating the anion. Further, the nitrogen atom on the pyridine ring of **1** is participating in two C–H···N hydrogen bonds ($d_{H\cdots N}$ = 2.714 Å, $\theta_{C\text{-}H\cdots N}$ = 167.18°; $d_{H\cdots N}$ = 2.737 Å, $\theta_{C\text{-}H\cdots N}$ = 135.95°), linking **1** to the phosphonium cation of **a**.

Cocrystal **1d** features a **1**···Br$^-$···**1** discrete halogen bonded dimer involving one crystallographically unique molecule of **1** ($d_{I\cdots Br}$ = 3.2924(10) Å, $\theta_{C\text{-}I\cdots Br}$ = 177.9(3)°), with an angle of $\theta_{I\cdots Br\cdots I}$ = 99.2° between the two halogen bonded fragments. In contrast to structure **1a**, the bromide anion displays no other close contacts and the nitrogen atom on the pyridine ring of **1** does not participate in hydrogen bonding. However, the proton in the *para* position relative to the nitrogen of **1** is participating in a H···C contact to the cation of **d** ($d_{H\cdots C}$ = 2.855 Å), reflecting the same contact as observed in structure **1a**. The overall crystal packing, shown in Figure 3, reveals a cation of **d** surrounded by the halogen bonded dimer in a unique square pattern exhibiting tetragonal symmetry. These patterns are stacked amongst each other, forming the crystal.

The crystal structure of **1e** features a large unit cell volume of 8263(12) Å^3, containing two molecules of PPNCl, two molecules of **1**, two water molecules, and two acetonitrile

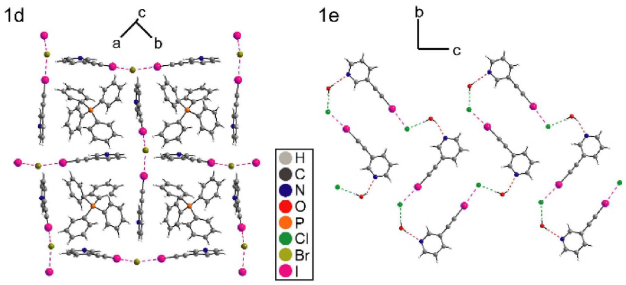

Figure 3. Depiction of the crystal packing of structure **1d** (left), and the halogen/hydrogen bonded fragment observed in structure **1e** (right). The dashed magenta lines denote the halogen bonds, the dashed red lines denote the H···N hydrogen bonds, and the dashed green lines denote H···Cl contacts. The cation in **1e** is not shown for clarity.

molecules. As a result, there are two crystallographically independent chloride anions, with each anion participating in a halogen bond with **1** and a hydrogen bond involving a water molecule. Following the labelling scheme of the crystal structure, there are five contacts to Cl(1): a halogen bond ($d_{I\cdots Cl}$ = 3.060(3) Å, $\theta_{C\text{-}I\cdots Br}$ = 174.61(15)°) with **1**, a hydrogen bond with water ($d_{Cl\cdots H}$ = 2.313 Å), two short contacts to the proton of the cation ($d_{Cl\cdots H}$ = 2.935 Å; $d_{Cl\cdots H}$ = 2.948 Å), and a short contact to the proton of acetonitrile ($d_{Cl\cdots H}$ = 2.653 Å). In contrast, Cl(2) participates in three contacts: a halogen bond ($d_{I\cdots Cl}$ = 3.102(3) Å, $\theta_{C\text{-}I\cdots Br}$ = 174.43(15)°) to **1**, a hydrogen bond to water ($d_{Cl\cdots H}$ = 2.294 Å), and a short contact to the proton of the cation ($d_{Cl\cdots H}$ = 2.766 Å). In addition to the I···Cl halogen bonds, both molecules of **1** participate in a N···H hydrogen bond involving the nitrogen atom on the pyridine ring ($d_{N\cdots H}$ = 2.281 Å; $d_{N\cdots H}$ = 2.182 Å). Overall, the alternation of I···Cl halogen bonds and N···H hydrogen bonds with **1** creates a unique framework, with a depiction shown in Figure 3. While the acetonitrile molecules form short N···H contacts between the cation and nitrogen of acetonitrile in addition to a Cl···H contact to the chloride anion, they do not appear to have a significant contribution to the overall framework. The crystal packs in alternating layers of the cation and halogen bonded fragments, building the overall crystal structure of **1 e**.

2 b includes two molecules of **2** and one molecule of **b** in the asymmetric unit. In addition to a I···Br halogen bond ($d_{I\cdots Br}$ = 3.1974(8) Å, $\theta_{C\text{-}I\cdots Br}$ = 170.71(12)°), **2** dimerizes *via* bridging O–H···O hydrogen bonding of the carboxylic acid groups, forming a Br···**2**···**2**···Br motif. The coordination sphere surrounding the Br^- anion includes two halogen bonds in a nearly linear configuration ($\theta_{I\cdots Br\cdots I}$ = 170.5°), in addition to three H···Br contacts involving the cation **b**. Both molecules of **2** in the hydrogen bonded dimer remain in the same molecular plane. However, the molecular plane of the hydrogen-bonded dimers alternate at right angles between the halogen bonding linkers, forming a 3D zig-zag motif.

The crystal structure of compound **2 c** exhibits a 1:1 molar ratio, in contrast to the 2:1 ratio observed in structure **2 b**. Despite this difference in the stoichiometry, the molecules of **2** participate in a I···Br halogen bond ($d_{I\cdots Br}$ = 3.1662(5) Å, $\theta_{C\text{-}I\cdots Br}$ = 175.12(10)°) in addition to hydrogen bonding. In this case, however, the angle between both halogen bonds is $\theta_{I\cdots Br\cdots I}$ = 102.88°, with the overall motif consisting of a zig-zag pattern, shown in Figure 2. This pattern generates space between the halogen/hydrogen bonded fragments, which is occupied by the cation. In addition to the two C–I···Br^- halogen bonds, the bromide anion is participating in five H···Br^- contacts involving the cation. Further, the cation displays disorder between the cyclopentyl group and a phenyl group.

Cocrystal **2 e** features one molecule of **2**, one molecule of **e**, and one molecule of acetonitrile in the asymmetric unit. Each molecule of **2** participates in a I···Cl halogen bond ($d_{I\cdots Br}$ = 3.1187(13) Å, $\theta_{C\text{-}I\cdots Br}$ = 173.37(13)°), in addition to a H···Cl hydrogen bond ($d_{H\cdots Cl}$ = 2.239 Å) rather than forming dimers *via* O–H···O hydrogen bonding as observed in structures **2 b** and **2 c**. As a result, a unique dimer is formed *via* both halogen and hydrogen bonds. In addition to a hydrogen bond and halogen bond, the chloride anion participates in a contact involving the proton of a nearby acetonitrile molecule. Much like structure **1 e**, structure **2 e** packs in alternating layers of the cation and halogen bonded fragments.

The halogen bond lengths observed in these structures, summarized in Table 1, are of the same order as previously reported structures featuring the iodoethynyl group coordinating halogen anions. For instance, the halogen bond lengths reported for the donor 1,3,5-tri(iodoethynyl)-2,4,6-trifluorobenzene coordinating a bromide anion are on the order of 3.1893(7) Å to 3.335(2) Å.[36] In contrast with our previous study on cocrystals featuring **2** with a series of nitrogen-containing heterocycles, the C–I···N halogen bond length varied between 2.741(6) Å to 3.021(3) Å,[44] notably shorter than the C–I···Br^- distances observed herein. Further X-ray crystallographic details are given in Table 2 and in the Supporting Information.

Table 1. Halogen bond geometry of the cocrystals investigated herein.

compound	XB moiety	XB length ($d_{I\cdots Y}$)/Å	R_{XB}[a]	XB angle $\theta_{C\text{-}I\cdots Y}$ (°)
1 a	C–I···Br^-	3.1344(9)	0.82	171.12(10)
1 d	C–I···Br^-	3.2924(10)	0.86	177.9(3)
1 e	C–I···Cl^-	3.060(3)	0.82	174.61(15)
	C–I···Cl^-	3.102(3)	0.83	174.43(15)
2 b	C–I···Br^-	3.1974(8)	0.83	170.71(12)
2 c	C–I···Br^-	3.1662(5)	0.83	175.12(10)
2 e	C–I···Cl^-	3.1187(13)	0.84	173.37(13)

[a] The normalized distance parameter was calculated using $R_{XB} = \frac{d_{I\bullet\bullet\bullet Y}}{\sum d_{vdW}}$ where Σd_{vdW} denotes the sum of the van der Waals radii.

Comparing the halogen bond donors **1** and **2**, it is noted that the nitrogen on the pyridine ring and the carboxylic acid functional groups have contrasting roles in the overall crystal structures. Whereas the carboxylic acid of **2** favoured dimerization *via* hydrogen bonding and formed continuous frameworks, the pyridine group of **1** favoured the formation of discrete halogen-bonded fragments. This is most clearly observed in structures **1 a** and **1 d**, while the continuous framework observed in **1 e** is a result of presence of a water molecule rather than the halogen bond donor or acceptor. Consequently, the halogen bond donor **2** may be a more versatile compound for engineering cocrystals, allowing for a more robust design of halogen bonded frameworks. Conversely, the basicity of the pyridine ring on **1** carries the benefits of self-assembly and the opportunity to form halide salts, which has also been mentioned in our previous report.[43]

2.2. ^{13}C Solid-State NMR Spectroscopy

Shown in Figure 4 are the ^{13}C SSNMR spectra of the cocrystals and precursors studied herein. The spectra of **1** and **2** have been previously reported.[43,44] The ^{13}C analysis yielded sufficient signal within a few hours for each compound, offering a quantitative comparison of the chemical shifts for both the halogen bond donor and the cation relative to the pure starting

Table 2. Selected single-crystal X-ray crystallographic data for **1a**, **1d**, **1e**, **2b**, **2c**, and **2e**.

compound	**1a**	**1d**	**1e**
empirical formula	$C_{27}H_{24}INPBr$	$C_{38}H_{28}I_2N_2PBr$	$C_{45}H_{39}IN_3OP_2Cl$
FW (g/mol)	600.25	877.30	862.08
crystal color	colourless	colourless	colourless
crystal size (mm)	0.50×0.30×0.20	0.625×0.347×0.308	0.10×0.10×0.10
crystal system	triclinic	tetragonal	monoclinic
crystal space group	$P\bar{1}$	$P\bar{4}2_1m$	$P2_1c$
T (K)	200(2)	200(2)	200(2)
a (Å)	9.789(2)	15.2918(12)	24.52(2)
b (Å)	10.949(2)	15.2918(12)	19.724(16)
c (Å)	12.974(3)	7.5919(6)	17.107(14)
α (°)	67.041(9)	90	90
β (°)	86.447(10)	90	92.882(17)
γ (°)	76.089(9)	90	90
V(Å^3)	1242.0(5)	1775.3(3)	8263(12)
Z	2	2	8
μ (mm^{-1})	2.977	2.970	0.955
F (000)	592	852	3504
Data collection			
Diffractometer	Bruker APEX-II CCD area detector diffractometer		
Absorption correction	Based on multi-scan		
No. of measured, independent and observed reflections	39758, 6792, 4935	82403, 2891, 1952	169474, 14971, 9526
R_{int}	0.0303	0.1328	0.1121
θ_{min} (°), θ_{max} (°)	1.706, 29.843	1.883, 30.925	0.831, 25.250
Refinement			
$R_{\_all}$, $R_{\_obs}$	0.0632, 0.0336	0.0903, 0.0403	0.0975, 0.0400
wR_{2_all}, wR_{2_obs}	0.0693, 0.0568	0.0853, 0.0683	0.1071, 0.0768
GooF	1.090	1.072	1.130
No. of parameters	281	115	969
No. of restraints	0	0	6
$\Delta\rho_{max}$, $\Delta\rho_{min}$ (e·Å^{-3})	1.430, −0.775	0.588, −0.862	0.721, −0.748
CCDC number	1909609	1909624	1909625
FW (g/mol)	929.32	955.36	887.08
crystal color	colourless	colourless	colourless
crystal size (mm)	0.10×0.10×0.10	0.10×0.10×0.10	0.10×0.10×0.10
crystal system	monoclinic	orthorhombic	monoclinic
crystal space group	$P2_1n$	$Pnma$	$P2_1n$
T (K)	200(2)	200(2)	200(2)
a (Å)	10.3558(2)	15.2297(4)	14.3122(6)
b (Å)	12.1985(3)	25.4689(9)	19.2273(9)
c (Å)	29.0810(6)	10.0477(3)	16.2184(7)
α (°)	90	90	90
β (°)	92.475(1)	90	109.846(1)
γ (°)	90	90	90
V(Å^3)	3670.24(14)	3897.3(2)	4198.0(3)
Z	4	4	4
μ (mm^{-1})	2.885	2.719	0.943
F (000)	1816	1872	1800
Data collection			
Diffractometer	Bruker APEX-II CCD area detector diffractometer		
Absorption correction	Based on multi-scan		
No. of measured, independent and observed reflections	60406, 9166, 5643	61724, 5005, 3272	75829, 10689, 6446
R_{int}	0.0681	0.0791	0.0635
θ_{min} (°), θ_{max} (°)	1.811, 28.369	2.179, 28.404	1.704, 28.634
Refinement			
$R_{\_all}$, $R_{\_obs}$	0.0860, 0.0354	0.0800, 0.0380	0.1016, 0.0402
wR_{2_all}, wR_{2_obs}	0.0789, 0.0625	0.0755, 0.0627	0.1150, 0.0812
GooF	1.018	1.094	1.127
No. of parameters	433	281	501
No. of restraints	0	104	0
$\Delta\rho_{max}$, $\Delta\rho_{min}$ (e·Å^{-3})	0.836, −0.669	0.694, −0.401	0.627, −1.179
CCDC number	1909626	1909627	1909628

Table 2. continued

compound	2b	2c	2e
empirical formula	$C_{39}H_{32}I_2O_4PBr$	$C_{41}H_{34}I_2O_4PBr$	$C_{47}H_{38}IN_2O_2P_2Cl$
FW (g/mol)	929.32	955.36	887.08
crystal color	colourless	colourless	colourless
crystal size (mm)	0.10×0.10×0.10	0.10×0.10×0.10	0.10×0.10×0.10
crystal system	monoclinic	orthorhombic	monoclinic
crystal space group	$P2_1n$	*Pnma*	$P2_1n$
T (K)	200(2)	200(2)	200(2)
a (Å)	10.3558(2)	15.2297(4)	14.3122(6)
b (Å)	12.1985(3)	25.4689(9)	19.2273(9)
c (Å)	29.0810(6)	10.0477(3)	16.2184(7)
α (°)	90	90	90
β (°)	92.475(1)	90	109.846(1)
γ (°)	90	90	90
V(Å^3)	3670.24(14)	3897.3(2)	4198.0(3)
Z	4	4	4
μ (mm^{-1})	2.885	2.719	0.943
F (000)	1816	1872	1800
Data collection			
Diffractometer	Bruker APEX-II CCD area detector diffractometer		
Absorption correction	Based on multi-scan		
No. of measured, independent and observed reflections	60406, 9166, 5643	61724, 5005, 3272	75829, 10689, 6446
R_{int}	0.0681	0.0791	0.0635
θ_{min} (°), θ_{max} (°)	1.811, 28.369	2.179, 28.404	1.704, 28.634
Refinement			
$R_{\_all}$, $R_{\_obs}$	0.0860, 0.0354	0.0800, 0.0380	0.1016, 0.0402
wR_{2_all}, wR_{2_obs}	0.0789, 0.0625	0.0755, 0.0627	0.1150, 0.0812
GooF	1.018	1.094	1.127
No. of parameters	433	281	501
No. of restraints	0	104	0
$\Delta\rho_{max}$, $\Delta\rho_{min}$ (e·Å^{-3})	0.836, −0.669	0.694, −0.401	0.627, −1.179

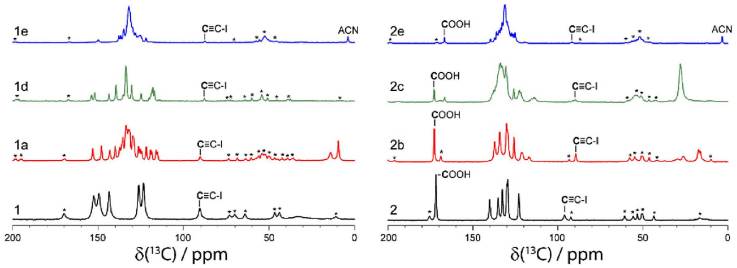

Figure 4. ^{13}C CP/MAS solid-state NMR spectra of the compounds investigated herein. The spectra of pure **1** and **2** were taken from previous reports.[43,44] The labels denote the carboxylic acid (**C**OOH), acetylene (**C**≡**C**–I), and acetonitrile (ACN) carbons. The asterisks denote spinning sidebands (ν_{MAS} = 8 kHz).

Table 3. ^{13}C chemical shifts of the compounds studied herein.

compound	XB moiety	δ(**C**OOH)/ ppm	δ(**C**≡**C**–I) ppm	δ(C–I)/ ppm
1[i]	C–I···N	n/a	90.5 ± 0.5[i]	32.6 ± 1.1[i]
1a	C–I···Br$^-$	n/a	90.3 ± 0.2	[a]
1d	C–I···Br$^-$	n/a	87.9 ± 0.1	[a]
1e	C–I···Cl$^-$	n/a	87.5 ± 0.1	31.3 ± 1.2
2[i]	C–I···C≡C	171.7 ± 0.1	96.0 ± 0.1	14.9 ± 0.4
2b	C–I···Br$^-$	172.7 ± 0.1	89.4 ± 0.1	[a]
2c	C–I···Br$^-$	172.8 ± 0.1	89.5 ± 0.8	[a]
2e	C–I···Cl$^-$	166.7 ± 0.1	91.7 ± 0.2	27.5 ± 2.3

[i] Chemical shifts of pure **1** and **2** have been reported elsewhere.[43,44]
[a] Resonance not observed due to breadth and low signal-to-noise.

materials. The chemical shifts of the carboxylic acid group (COOH), the acetylene carbon (C≡C–I), and the carbon covalently bonded to iodine (C–I) are summarized in Table 3. Although satisfactory signal was obtained for each spectrum, the carbon covalently bonded to iodine remained difficult to observe as a result of the breadth of the resonance, low signal intensity of the resonance, and spectral overlap from the cation in some cases. The signal intensity for the cocrystals in Figure 4 appears to be lower than that for the pure starting materials as a result of the higher intensity of the cation's ^{13}C signal. Overall, the chemical shift changes observed in Figure 4 support the occurrence of cocrystallization, while there is an absence of signal from any unreacted starting materials. Although solvent-based crystallizations were used to grow crystals suitable for

single crystal X-ray diffraction, the compounds studied here by SSNMR were analyzed directly from the mechanochemical preparations. As a result, mechanochemical ball milling appears to be a reliable route towards these unique halogen bonded compounds, and its combination with NMR crystallography can accelerate the discovery of novel halogen-bonded materials.

In comparison to their respective starting materials, the ^{13}C chemical shift of the acetylene carbon (C≡C–I) appears to be consistently lower in the cocrystals. For instance, there is a difference of 6.6 ± 0.1 ppm in the chemical shift of the acetylene carbon when comparing **2** to **2b**. Further, this decrease in the ^{13}C chemical shift is greater for cocrystals of **2** than for cocrystals of **1**. This may be a result of the starting material of **1** exhibiting a C–I···N halogen bond, while the starting material of **2** exhibits a weaker C–I···C≡C halogen bond coordinating the acetylene carbon. In contrast, the C–I chemical shift appears to increase when comparing **2** to **2e**, with a difference of 12.6 ± 2.3 ppm upon the formation of the cocrystals. This large increase contrasts with the comparison between **1** and **1e**, which saw an insignificant change in the chemical shift. This decrease in the ^{13}C chemical shift of the acetylene carbon and increase in the C–I carbon is in agreement with our previous reports for both compound **1** and compound **2**.[43,44]

In regards to the ^{13}C resonance of the carboxylic acid of series **2**, the chemical shift appeared to be overall sensitive to the hydrogen bonding motif exhibited in the crystal structure. In the compounds featuring an O–H···O hydrogen bond dimerization, the chemical shifts did not significantly change, with a slight increase of 1.1 ± 0.1 ppm when comparing **2** to compound **2c**. However, upon the formation of a O–H···Cl^- hydrogen bond, a significant decrease of 4.3 ± 0.2 ppm is observed. As a result, the ^{13}C chemical shift of the carboxylic acid may be an indicator to the nature of hydrogen bonding motif in the crystal structure. This appears to be in agreement with our previous results, where the formation of a O–H···N hydrogen bonding motif featuring **2** and a nitrogen-containing heterocycle yielded a decrease in the ^{13}C resonance of the carboxylic acid on the order of 3 ppm.

2.3. ^{31}P solid-state NMR Spectroscopy

Due to its higher sensitivity compared to ^{13}C, ^{31}P SSNMR boasts the advantage of more rapidly identifying excess starting material and the presence of side phases in mechanochemically prepared powders. Previously, ^{31}P SSNMR has been used to investigate pure phosphonium halide salts,[51] in addition to halogen-bonded cocrystals featuring phosphonium selenides and oxides, showing clear chemical shift changes upon cocrystallization.[42,52,53,54] The compounds reported herein were explored by ^{31}P SSNMR after their preparation by mechanochemical ball milling without further manipulations; spectra are shown in Figure 5. The ^{31}P chemical shifts of the halogen-bonded cocrystals were compared to chemical shifts of the pure halide salts, which may be found in Table 4. In these cases, there is a clear and unambiguous chemical shift difference between the pure phosphonium halide salts and their respective cocrystals, with each site in the asymmetric unit of the crystal structure having a unique chemical shift. Each spectrum required approximately 5 minutes to acquire.

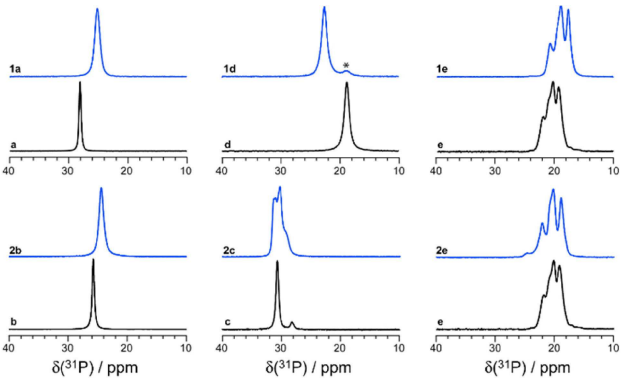

Figure 5. ^{31}P CP/MAS solid-state NMR spectra of the compounds investigated herein. The asterisk denotes the presence of a trace residual impurity of pure **d** in the spectrum of **1d**.

Table 4. ^{31}P chemical shifts of compounds studied herein.[a]

XB acceptor	δ(^{31}P)/ ppm	cocrystal	δ(^{31}P)/ ppm
a	28.1 ± 0.1	**1a**	25.2 ± 0.1
b	25.7 ± 0.1	**2b**	24.4 ± 0.1
c	30.7 ± 0.1	**2c**	31.1 ± 0.3
	28.2 ± 0.2		30.3 ± 0.1
d	18.8 ± 0.1	**1d**	22.6 ± 0.1

[a] Chemical shifts are not reported for **e**, **1e**, and **2e** due to the presence of multiple crystallographic sites and residual dipolar coupling to ^{14}N.

The ^{31}P SSNMR spectra of compounds **1a**, **1d**, and **2b** each consist of a single resonance, with a chemical shift difference between the pure halide salt and the cocrystal of 2.9 ± 0.1 ppm for compound **1a**. The ^{31}P SSNMR spectrum of **1d** revealed small (< 10%) amounts of unreacted starting material (**d**) remaining in the sample. The ^{31}P SSNMR spectrum of sample **2c** appears to have two resonances with a slight chemical shift difference of 0.8 ± 0.3 ppm. The presence of these two resonances could be due to the disorder present in the crystal structure, with the cyclopentyl group occupying the position of one of the phenyl groups. The integration of both ^{31}P resonances reveals a ratio of approximately 0.56:0.44, which is in agreement with the occupancy ratio derived from X-ray crystallography, 0.568(9):0.432(9). The asymmetric broadening and splitting of the ^{31}P SSNMR spectrum of **e** suggests residual dipolar coupling between ^{31}P and the directly bonded ^{14}N atom. Although a published single-crystal X-ray structure of **e** indicates a single crystallographically distinct phosphorus site,[55] the powder X-ray diffraction pattern of the sample used in our work does not match the pattern simulated based on the single-crystal structure (see Supporting Information). Our inability to simulate the ^{31}P SSNMR spectrum based on a single ^{31}P site coupled to ^{14}N further suggests that the polymorph used in this work differs from the previously reported one. Nevertheless,

resonance shifts upon cocrystallization are clear particularly for **1 e** (Figure 5 and Figure S14).

Overall, ^{31}P SSNMR is a sensitive spectroscopic tool to identify the occurrence of cocrystallization. With experimental times on the order of 5 minutes, and the chemical shift sensitive to the crystallographic environment, ^{31}P offers several advantages to the crystal engineer. In contrast, the ^{13}C SSNMR required several hours to perform, and yields spectra with multiple resonances. As a result, the ^{13}C spectrum may be more ambiguous to interpret, especially with smaller chemical shift differences between the starting materials and the cocrystals. Nevertheless, ^{13}C SSNMR remains applicable to most organic compounds, while ^{31}P SSNMR obviously requires the presence of phosphorus in the sample.

2.4. Powder X-Ray Diffraction

As mentioned above, the mechanochemical ball milling results in a fine crystalline powder which could be analysed via powder X-ray diffraction. The resulting diffractograms can be compared to the calculated powder patterns generated from the crystal structure obtained via SCXRD. This analysis, combined with SSNMR, can quickly confirm the formation of the wanted cocrystal and also the formation of polymorphs in the resulting powders (see Supporting Information). The products from mechanochemical ball milling have been analysed without any purification. Shown in Figure 6 is an example of an experimental diffractogram for **1 e** along with the simulation generated from the single-crystal data. All other powder X-ray diffractograms are shown in the Supporting Information.

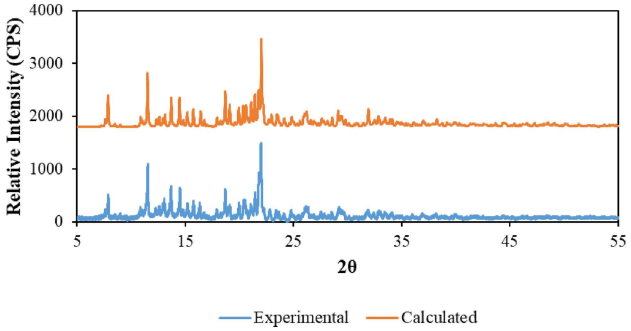

Figure 6. Experimental and calculated powder X-ray diffractograms of **1 e**, (3-iodoethynylpyridine)$_2$(bis[triphenylphosphoranylidene]ammonium chloride)$_2$(H_2O)$_2$(ACN)$_2$.

3. Conclusions

The production of cocrystals of **1** and **2** with a series of halide salts was successfully performed by mechanochemistry, confirmed by both X-ray crystallography and multinuclear solid-state magnetic resonance spectroscopy. Across all six reported structures, a halogen bond has been observed between the iodine on the iodoacetylene group and the halide ion (Br^-, Cl^-). The cocrystals featuring **1** favoured discrete entities with the basic nitrogen on the pyridine ring acting as a hydrogen bond acceptor. In contrast, cocrystals built with **2** featured both hydrogen bonded dimers and C–I···X^- halogen bonds. The use of ^{31}P solid-state NMR allowed for a rapid confirmation for the occurrence of halogen bond-induced cocrystallization, while ^{13}C solid-state NMR was a reliable indicator for the occurrence of both halogen bonding and hydrogen bonding motifs.

Supporting Information Available

CIFs, powder X-ray diffractograms, further experimental details. For full diffraction datasets, refer to CCDC numbers 1909609 (**1 a**), 1909624 (**1 d**), 1909625 (**1 e**), 1909626 (**2 b**), 1909627 (**2 c**), 1909628 (**2 e**).

Acknowledgements

PMJS and DLB thank the Natural Sciences and Engineering Research Council of Canada for a scholarship and for research funding, respectively.

Conflict of Interest

The authors declare no conflict of interest.

Keywords: halogen bonding · hydrogen bonding · solid-state NMR · crystal engineering · X-ray crystallography

[1] S. Abe, H. Tabe, H. Ijiri, K. Yamashita, K. Hirata, K. Atsumi, T. Shimoi, M. Akai, H. Mori, S. Kitagawa, T. Ueno, *ACS Nano* **2017**, *11*, 2410–2419.
[2] M. Lusi, *Cryst. Growth Des.* **2018**, *18*, 3704–3712.
[3] M. A. Haque, A. N. Gandi, R. Mohanraman, Y. Weng, B. Davaasuren, A.-H. Emwas, C. Combe, D. Baran, A. Rothenberger, U. Schwingenschlögl, H. N. Alshareef, S. Dong, T. Wu, *Adv. Funct. Mater.* **2019**, *29*, 1809166.
[4] T. Murata, C. Yamada, K. Furukawa, Y. Morita, *Communications Chemistry*, **2018**, *1*, 47.
[5] C. B. Aakeroy, N. R. Champness, C. Janiak, *CrystEngComm*, **2010**, *12*, 22–43.
[6] G. R. Desiraju, *Angew. Chem. Int. Ed. Engl.* **1995**, *34*, 2311–2327.
[7] E. Grothe, H. Meekes, E. Vlieg, J. H. ter Horst, R. de Gelder, *Cryst. Growth Des.* **2016**, *16*, 3237–3243.
[8] S. Aitipamula *Cryst. Growth Des.* **2012**, *12*, 2147–2152.
[9] D. R. Weyna, T. Shattock, P. Vishweshwar, M. J. Zaworotko, *Cryst. Growth Des.* **2009**, *9*, 1106–1123.
[10] J.-L. Do, T. Friščić, *Synlett* **2017**, *28*, A-AA.
[11] G. A. Bowmaker, *Chem. Commun.* **2013**, *49*, 334–348.
[12] P. M. J. Szell, S. A. Gabriel, E. Caron-Poulin, O. Jeannin, M. Fourmigué, D. L. Bryce, *Cryst. Growth Des.* **2018**, *18*, 6227–6238.
[13] A. Mukherjee, S. Tothadi, G. R. Desiraju, *Acc. Chem. Res.* **2014**, *47*, 2514–2524.
[14] C. B. Aakeröy, T. K. Wijethunga, J. Desper, *J. Mol. Struct.* **2014**, *1072*, 20–27.
[15] P. Metrangolo, H. Neukirch, T. Pilati, G. Resnati, *Acc. Chem. Res.* **2005**, *38*, 386–395.
[16] P. Politzer, J. S. Murray, *Crystals.* **2017**, *7*, 212–226.
[17] T. Clark, M. Hennemann, J. S. Murray, P. Politzer, *J. Mol. Model.* **2007**, *13*, 291–296.

[18] P. Politzer, J. S. Murray, T. Clark, G. Resnati, *Phys. Chem. Chem. Phys.* **2017**, *19*, 32166–32178.
[19] G. R. Desiraju, P. S. Ho, L. Kloo, A. C. Legon, R. Marquardt, P. Metrangolo, P. Politzer, G. Resnati, K. Rissanen, *Pure Appl. Chem.* **2013**, *85*, 1711–1713.
[20] K. E. Riley, J. S. Murray, J. Fanfrlík, J. Řezáč, R. J. Solá, M. C. Concha, F. M. Ramos, P. Politzer, *J. Mol. Model.* **2011**, *17*, 3309–3318.
[21] K. E. Riley, J. S. Murray, J. Fanfrlík, J. Řezáč, R. J. Solá, M. C. Concha, F. M. Ramos, P. Politzer, *J. Mol. Model.* **2013**, *19*, 4651–4659.
[22] C. B. Aakeröy, T. K. Wijethunga, J. Desper, M. Đaković, *Cryst. Growth Des.* **2015**, *15*, 3853–3861.
[23] C. B. Aakeröy, D. Welideniya, J. Desper, *CrystEngComm.* **2017**, *19*, 11–13.
[24] L. González, N. Gimeno, R. M. Tejedor, V. Polo, M. Blanca Ros, S. Uriel, J. L. Serrano, *Chem. Mater.* **2013**, *25*, 4503–4510.
[25] H. M. Yamamoto, R. Maeda, J.-I. Yamaura, R. Kato, *J. Mater. Chem.* **2001**, *11*, 1034–1041.
[26] L. Turunen, F. Pan, N. K. Beyeh, J. F. Trant, R. H. A. Ras, K. Rissanen, *Cryst. Growth Des.* **2018**, *18*, 513–520.
[27] C. A. Gunawardana, M. Đaković, C. B. Aakeröy, *Chem. Commun.* **2018**, *54*, 607–610.
[28] C. Laurence, M. Queignec-Cabanetos, T. Dziembowska, R. Quiegnec, B. Wojtkowiak, *J. Am. Chem. Soc.* **1981**, *103*, 2567–2573.
[29] L. Luo, C. Wilhelm, A. Sun, C. P. Grey, J. W. Lauher, N. S. Goroff, *J. Am. Chem. Soc.* **2008**, *130*, 7702–7709.
[30] C. Perkins, S. Libri, H. Adams, L. Brammer, *CrystEngComm* **2012**, *14*, 3033–3038.
[31] N. S. Goroff, S. M. Curtis, J. A. Webb, F. W. Fowler, J. W. Lauher, *Org. Lett.* **2005**, *7*, 1891–1893.
[32] M. Fourmigué, *Acta Crystallogr.* **2017**, *B73*, 138–139.
[33] J. Grebe, G. Geiseler, K. Harms, K. Dehnicke, *Z. Naturforsch.* **1999**, *54b*, 77–86.
[34] M. C. Pfrunder, A. S. Micallef, L. Rintoul, D. P. Arnold, J. McMurtrie, *Cryst. Growth Des.* **2016**, *16*, 681–695.
[35] J. Lieffrig, O. Jeannin, M. Fourmigué, *J. Am. Chem. Soc.* **2013**, *135*, 6200–6210.
[36] P. M. J. Szell, B. Gabidullin, D. L. Bryce, *Acta Crystallogr.* **2017**, *B73*, 153–162.
[37] A. Brown, P. D. Beer, *Chem. Commun.* **2016**, *52*, 8645–8658.
[38] J. Y. C. Lim, I. Marques, V. Félix, P. D. Beer, *J. Am. Chem. Soc.* **2017**, *139*, 12228–12239.
[39] D. Cinčić, T. Friščić, W. Jones, *J. Am. Chem. Soc.* **2008**, *130*, 7524–7525.
[40] K. Lisac, V. Nemec, F. Topić, M. Arhangelskis, P. Hindle, R. Tran, I. Huskić, A. J. Morris, T. Friščić, D. Cinčić, *Cryst. Growth Des.* **2018**, *18*, 2387–2396.
[41] D. Cinčić, T. Friščić, W. Jones, *Chem. Eur. J.* **2008**, *14*, 747–753.
[42] Y. Xu, J. Viger-Gravel, I. Korobkov, D. L. Bryce, *J. Phys. Chem. C* **2015**, *119*, 27104–27117.
[43] P. M. J. Szell, G. Cavallo, G. Terraneo, P. Metrangolo, B. Gabidullin, D. L. Bryce, *Chem. Eur. J.* **2018**, *24*, 11364–11376.
[44] P. M. J. Szell, J. Dragon, S. Zablotny, S. R. Harrigan, B. Gabidullin, D. L. Bryce, *New J. Chem.* **2018**, *42*, 10493–10501.
[45] APEX 2, Bruker AXS Inc., Madison, Wisconsin, USA, 2012.
[46] G. M. Sheldrick, SADABS, Program for empirical absorption correction of area detector data, University of Göttingen, Germany, 1996.
[47] G. M. Sheldrick, *Acta Crystallogr.* **2015**, *C71*, 3–8.
[48] L. J. Farrugia, *J. Appl. Crystallogr.* **1999**, *32*, 837–838.
[49] L. J. Farrugia, *J. Appl. Crystallogr.* **2012**, *45*, 849–854.
[50] A. L. Spek, *Acta Crystallogr.* **2009**, *D65*, 148–155
[51] K. M. N. Burgess, I. Korobkov, D. L. Bryce, *Chem. Eur. J.* **2012**, *18*, 5748–5728.
[52] Y. Xu, L. Champion, B. Gabidullin, D. L. Bryce, *Chem. Commun.* **2017**, *53*, 9930–9933.
[53] J. Viger-Gravel, J. E. Meyer, I. Korobkov, D. L. Bryce, *CrystEngComm.* **2014**, *16*, 7285–7297.
[54] Y. Xu, J. Huang, B. Gabidullin, D. L. Bryce, *Chem. Commun.* **2018**, *54*, 11041–11043.
[55] C. Knapp, R. Uzun, *Acta Crystallogr.* **2010**, *E66*, o3185.

Manuscript received: June 3, 2019
Revised manuscript received: August 12, 2019